PFC/RR-91-1

SAFETY AND PROTECTION FOR LARGE-SCALE MAGNET SYSTEMS – FY90 REPORT

R.J. Thome, R.D. Pillsbury, Jr., J.R. Hale,
W.R. Mann, A. Shajii

January 1991

Plasma Fusion Center
Massachusetts Institute of Technology
Cambridge, Massachusetts 02139

Submitted to
Idaho National Engineering Laboratory
Idaho Falls, Idaho

This work was supported in part under EG&G Subcontract # C88-110982-TKP-154-87

Table of Contents

List of Figures

List of Tables

MIT Plasma Fusion Center
FY90 Safety and Protection Annual Report

1.0 Introduction

In FY89, an Engineers/Masters thesis was completed[1] which included a code for adiabatic quench propagation analysis in multiple, superconducting coils. In FY90, this material was presented at the 1990 Applied Superconductivity Conference[2] and the code was expanded and applied to another experimental test case. In addition, the capabilities of selected stability codes for internally cooled cabled superconductors were reviewed. Zero and one-dimensional codes were selected for study and application to selected cases for initial evaluation.

The modifications to the adiabatic quench code include: 1) the ability to initiate normal regions due to temperature rise from passive materials in close proximity to portions of the superconducting winding which are remote from the initially propagating normal zone, 2) the capability to plot temperature contours within the winding at selected instants of time, and 3) the ability to compute the local inductive voltage component within the winding so that this can be combined with the local resistive voltage to get the net voltage distribution along the conductor in the magnet.

The test case to which the quench code was applied[3] involved a superconducting solenoid with winding mandrel sections which were sufficiently conducting to carry significant induced currents during a quench and initiate normal regions at sections remote from the initially normal zone. Comparisons were made of the measured and computed current vs time profiles for the coil and with the maximum measured temperature. Agreement with the experimental results was very good.

During FY90 we also reviewed existing codes at MIT for internally cooled cabled superconductor analysis and selected two to "exercise" for possible future modification and use in a quench propagation code. This activity will continue in FY91. The change to quench analysis is nontrivial for this type of conductor because most codes are stability oriented and this is typically determined on a time scale of 1-10 ms, requiring substantial computational time. Quench details, on the other hand, evolve over 10s of seconds to minutes; hence, models must be researched and incorporated which can handle the longer time scale without prohibitive computer power or time. This report describes features of the two codes which were selected.

[1] M. Oshima, "Computation of Quench Propagation in Multiple Superconducting Coils,"

Engineers/MS Thesis, MIT Dept of Nuclear Engineering, January 1990.

[2] M. Oshima, R.J. Thome, W.R. Mann, and R.D. Pillsbury, "PQUENCH-A 3D Quench Propagation Code Using A Logical Coordinate System," presented at 1990 Applied Superconductivity Conference, Oak Brook, IL, Sept, 1990, to bbe published, *IEEE Trans. Mag.*, Mar.1991.

[3] D.J. Waltman, M.J. Superczynski, and F.E. McDonald, "Design, Construction, and Test of a 0.61 meter Diameter, Epoxy Impregnated Superconductive Magnet," DTNSRDC/PA 81/18, Oct, 1983.

2.0 Modifications to Adiabatic Quench Code

2.1 Code Capabilities

The structure and capabilities of the code as originally written can be found in the first two references listed at the end of the previous section. This section presents capabilities following selected modifications and section 2.1 shows the results of the code application, in FY90, to some experimental data.

In FY90 the adiabatic quench code was modified so that it now includes the following list of key features:

- Normal fronts can propagate along and transverse to the conductor;
- Material properties are functions of magnetic field and temperature;
- Magnetic field and temperature are updated locally at all points as the transient progresses;
- Multiple normal fronts can be propagated; they can be initiated by thermal conduction through material adjacent to an existing normal zone or by inducing currents in passive material adjacent to the winding which then becomes sufficiently warm to start a normal front in the nearby winding;
- Multiple inductively coupled circuits can be treated during the transient;
- Output from the code includes the current transients in the circuits as well as the local temperature and voltage distributions; recent modifications include the ability to plot temperature contours within the winding section at a specified time.

2.2 Comparison with Experiment

During FY90 the code was modified somewhat and used to analyze quench propagation in a solenoid described in the last reference at the end of section 1.0. A section through

the superconducting solenoid is shown in Figure 2-1. The dashed lines show the location of passive structural elements which are electrically conducting. They are axially symmetric with the solenoid and capable of carrying an induced current as the current in the main coil changes. The induced current heats the passive elements and under some circumstances, can be sufficient to start new normal zones in the adjacent winding sections before they would usually be driven normal by the initial normal front. The result is a somewhat faster transient and distribution of the energy dissipated over a larger volume of winding.

Figure 2-2 shows field lines generated by the superconducting coil at its operating current level. It indicates the large amounts of flux linked by the passive elements which can then induce currents in the elements as the field changes. Figure 2-3 shows contours of constant field magnitude at the operating current level. Field coefficients per unit current in the main coil and in the passive elements are stored by the code and used at each point in the transient to determine the local field magnitude for use in material property determination (e.g., electrical resistivity at each point in each normal zone).

In Figure 2-4, the computed and measured current vs time transients for the main coil are compared for a quench from the operating current of 150 A. No adjustments to material properties and no adjustable parameters were used in the computation. Hence, the agreement is considered to be quite good.

Figure 2-5 is a graph of the local temperature vs element number at $t=2\times10^{-3}$ s. Elements are numbered along the wire in the coil from the inside to the outside. At this instant the quench has just started at a point on the inside layer corresponding to the maximum field magnitude. Similar plots are shown in Figures 2-6 and 2-7 for times of 50 ms and 150 ms, respectively. This shows the "usual" progression of a normal zone along the wire as well as initiation of normal zones in adjacent layers in that each spike corresponds to a separate propagating normal zone triggered by transverse propagation.

Figure 2-8 is similar to the previous plots, but is for t=200 ms and also shows a large number of additional normal zones started at the high numbered elements which are located near the passive components near the outer diameter of the superconducting winding. Some of the intermediate spikes in the midrange element numbers correspond to winding sections adjacent to passive elements at the bottom of the assembly in Figure 2-1. Triggering the large number of additional normal zones tends to distribute the energy more uniformly through the winding and leads to a faster transient. Computational tests in which triggering by passive elements was suppressed did not lead to good agreement between the measured and computed current transients.

Figures 2-9 through 2-11 show similar plots at later instants of time and indicate the continued increase in winding temperature as the transient progresses. Most of the energy

is dissipated by 1.2 s. Figure 2-11 shows a maximum temperature at this time of about 109 K. The measured maximum temperature was 119 K. This is considered to be good agreement.

Figures 2-12 and 2-13 show computed contours of constant temperature in the winding at 400 ms and 1.2 s, respectively. The sawtooth nature of the contours is due to the coarseness of the grid over which field magnitudes are considered constant at any given instant for the purposes of computing material properties. This is believed to be a reasonable approximation to save computer time. Temperature variations are determined on a much finer grid since they have a stronger influence.

The voltage distribution in the winding is nonuniform and varies with time. Figure 2-14 shows the resistive and inductive components of the voltage at 150 ms as well as the net voltage distribution.

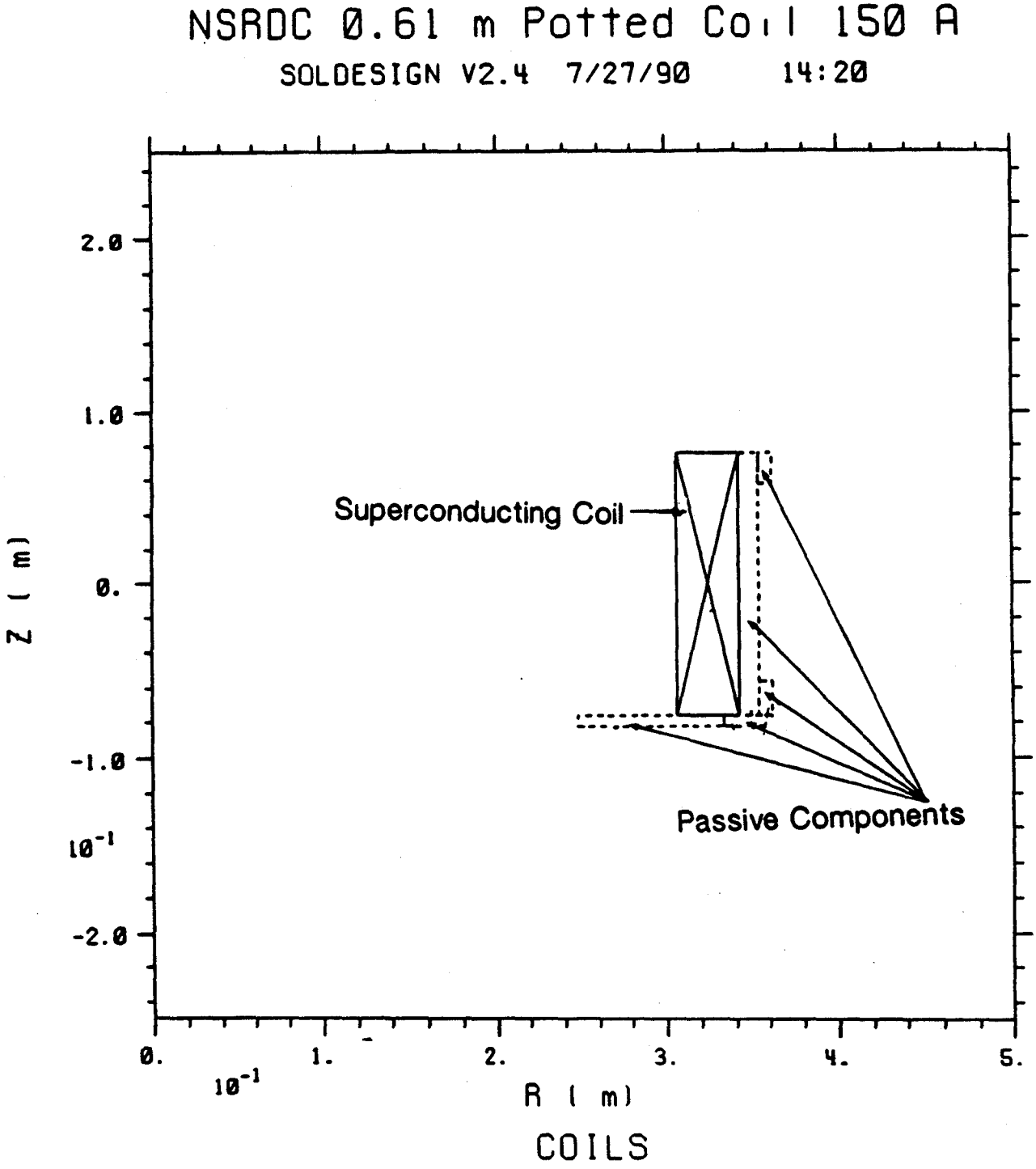

Figure 2–1
Section of Superconducting Coil and Conducting Elements Near the Winding

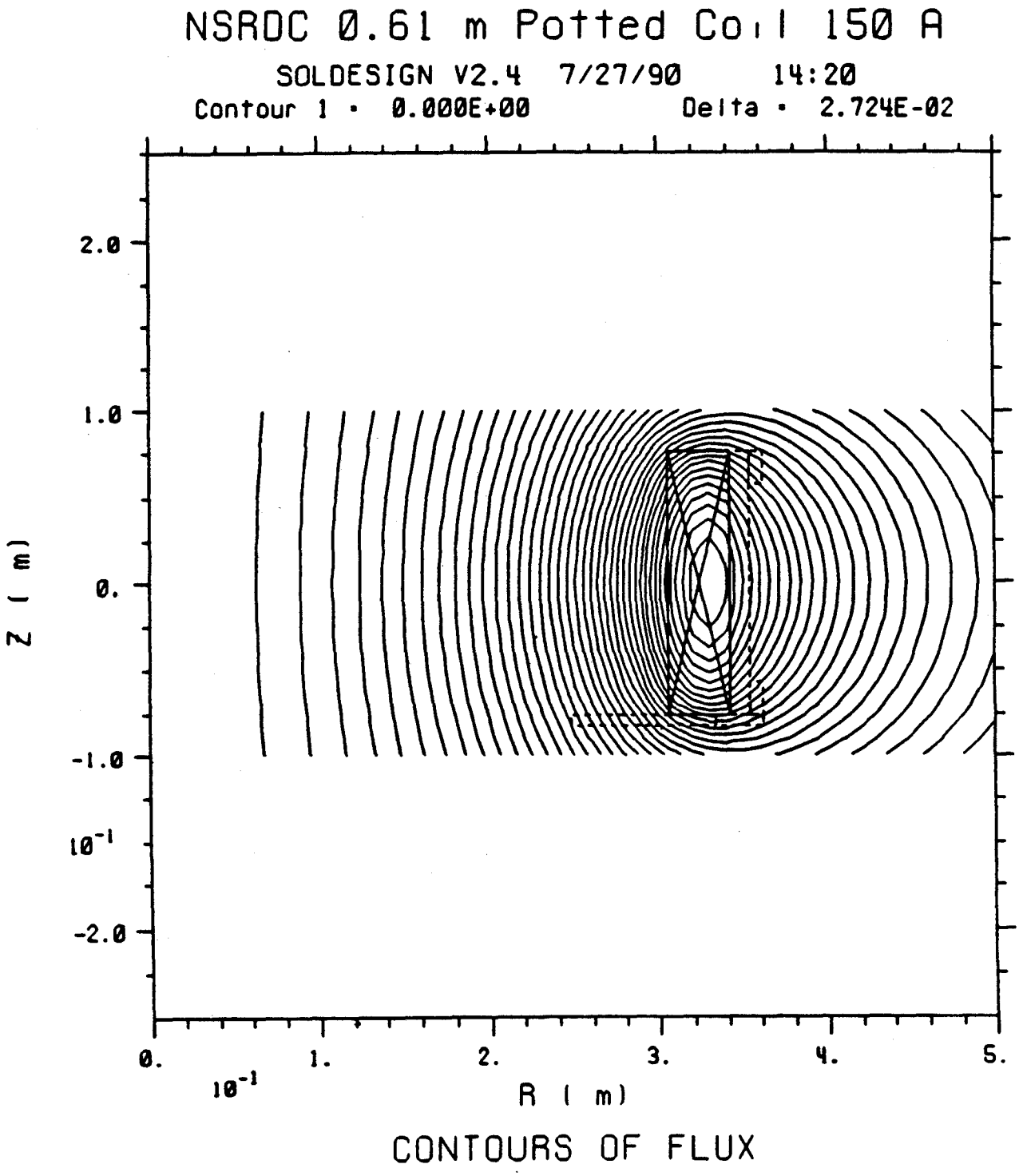

Figure 2–2
Magnetic Field Lines Generated by the Superconducting Coil at Operating Current

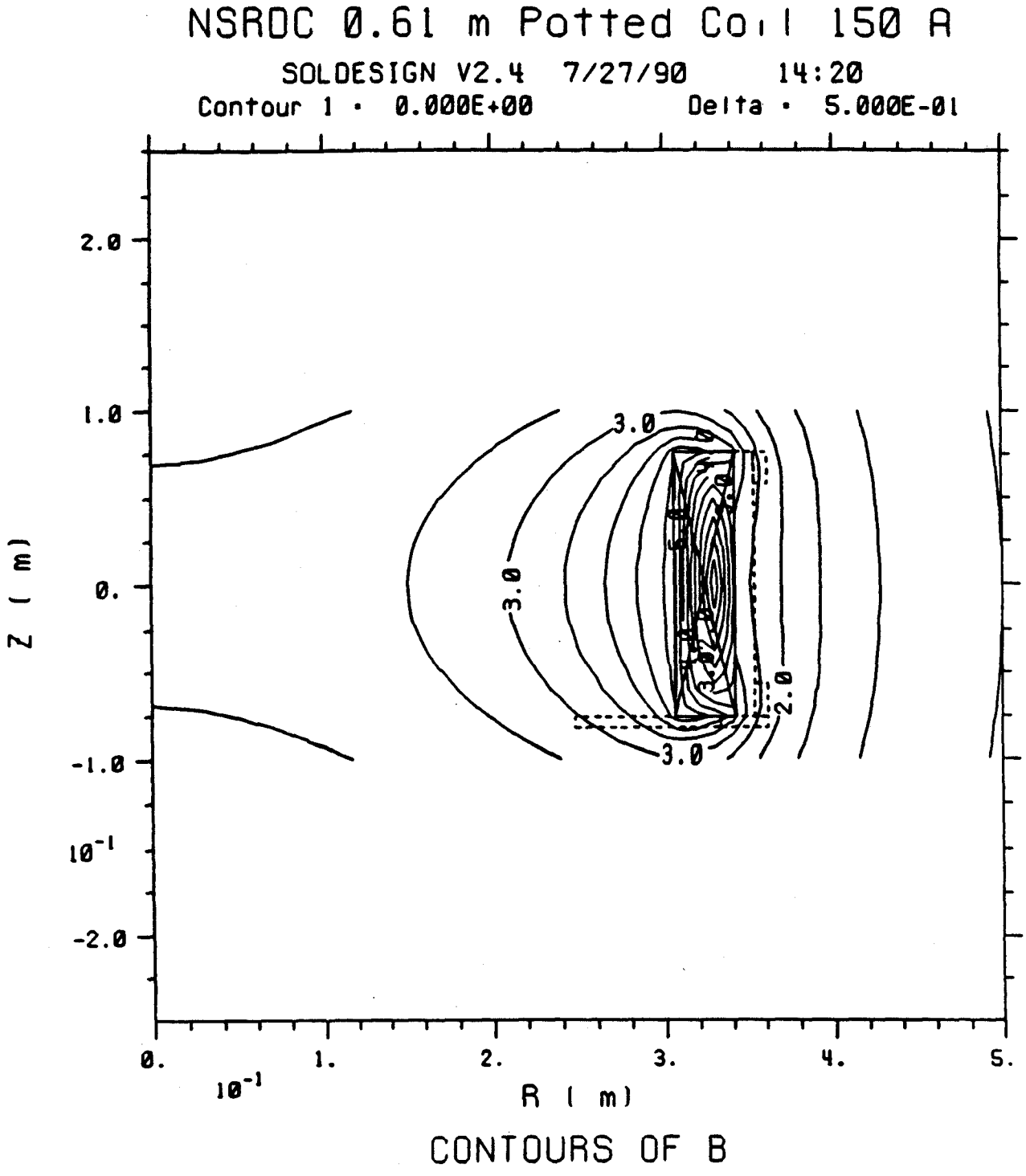

Figure 2–3
Contours of Constant Field Magnitude at the Operating Current

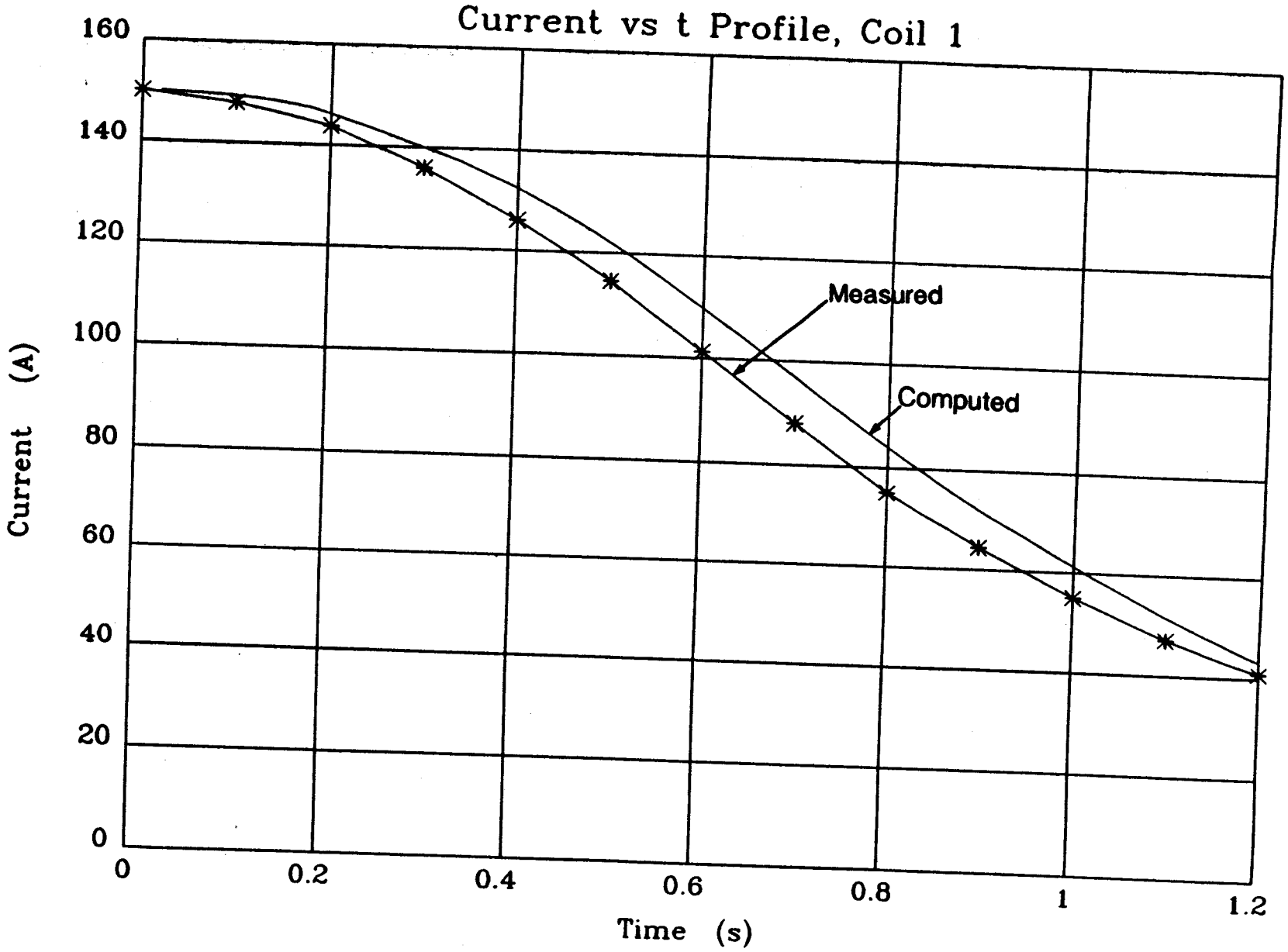

Figure 2–4

Comparison of Calculated and Measured Current Transients for the Main Coil During Quench

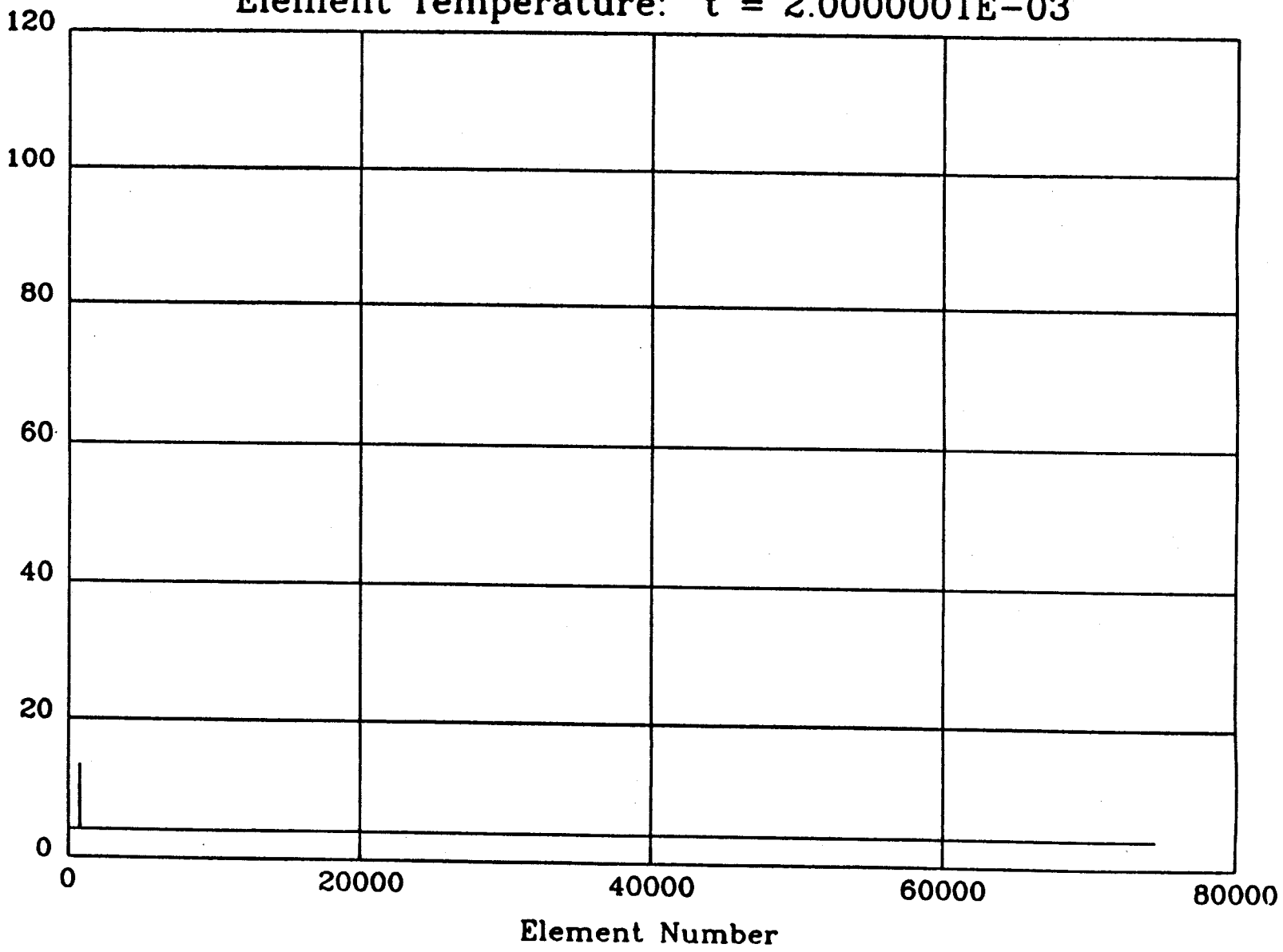

Figure 2–5
Local Temperature vs Element Number at t = 2×10^{-3} s

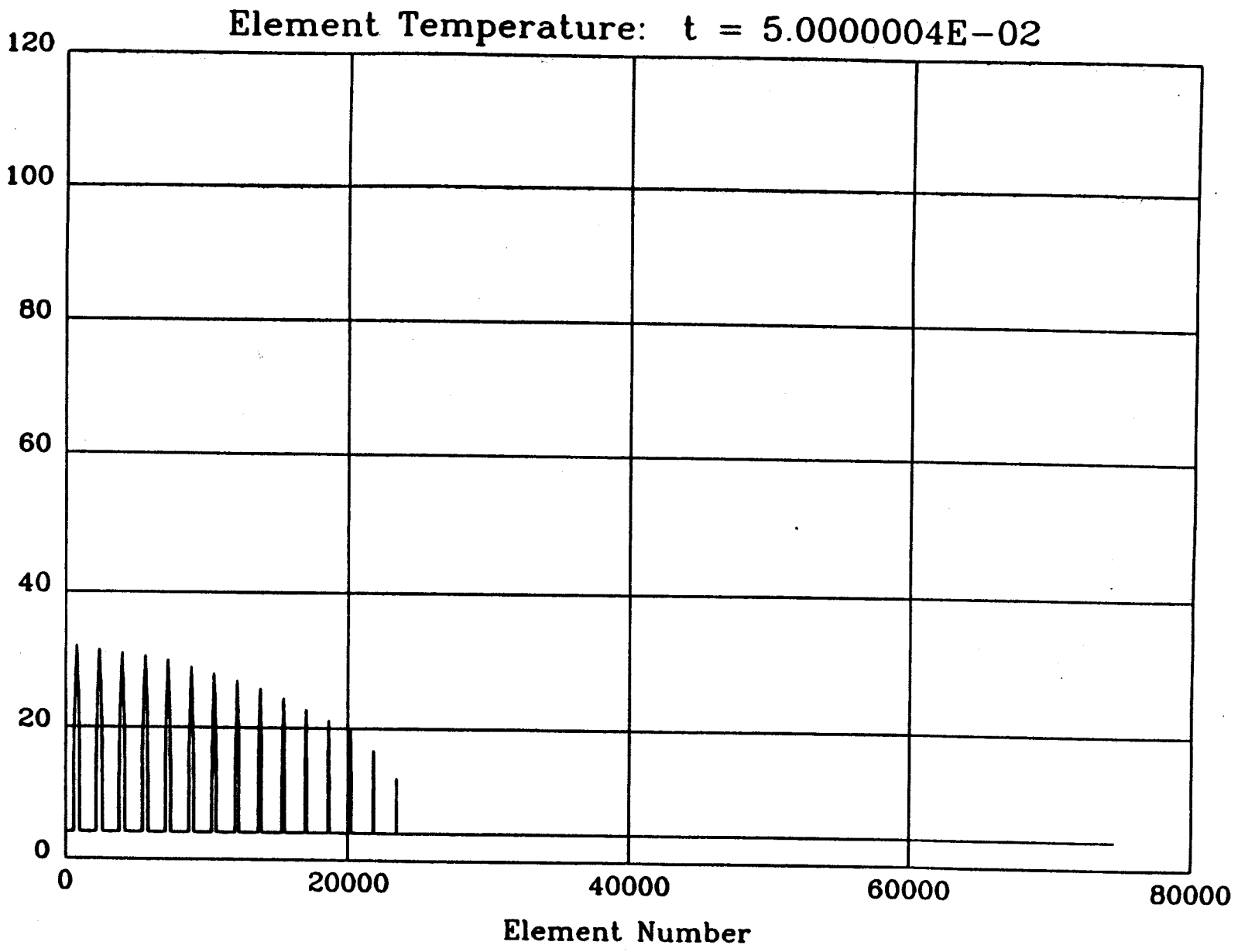

Figure 2–6
Local Temperature vs Element Number at t = 50 ms

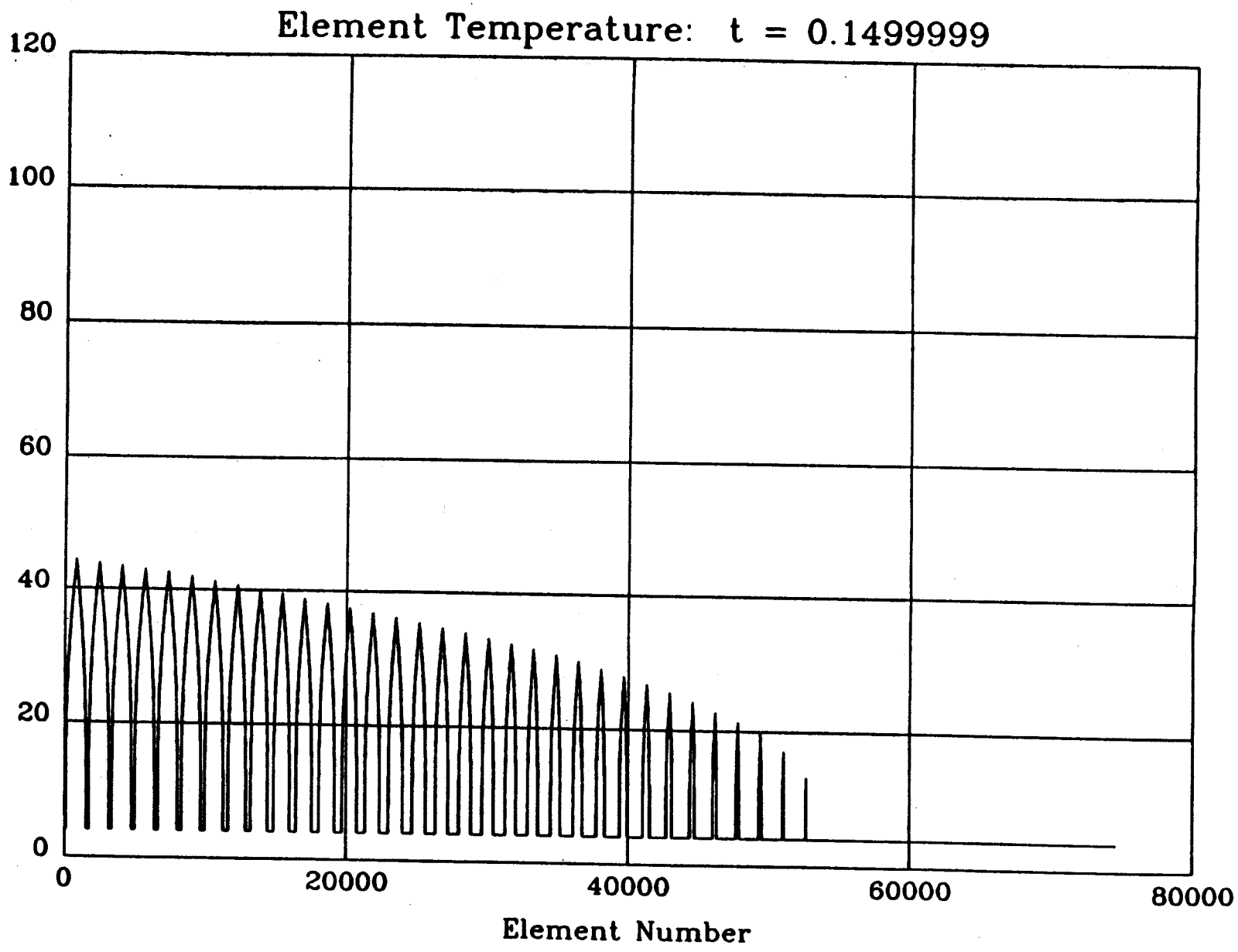

Figure 2–7
Local Temperature vs Element Number at t = 150 ms

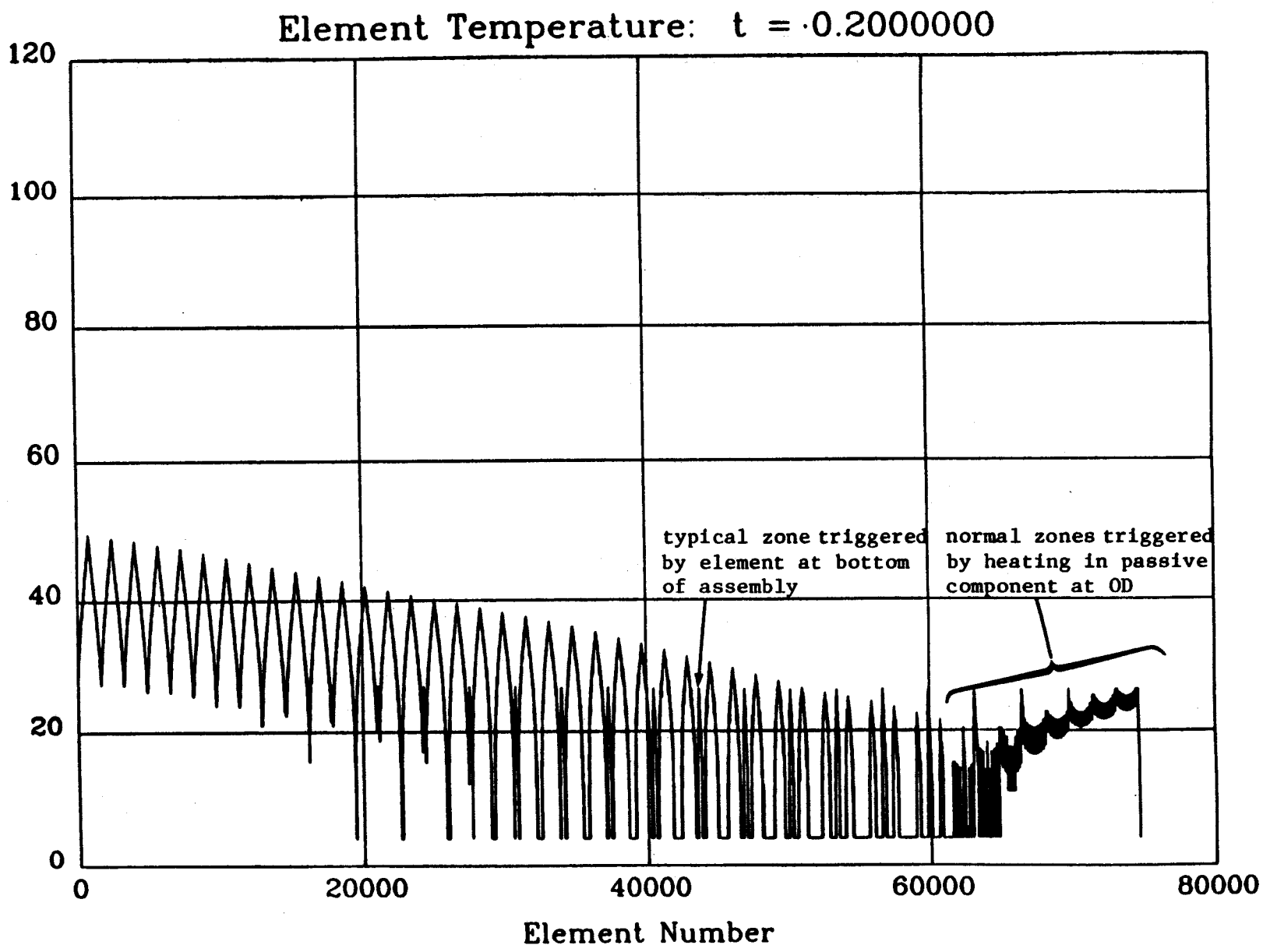

Figure 2–8
Local temperature vs Element Number at t = 200 ms

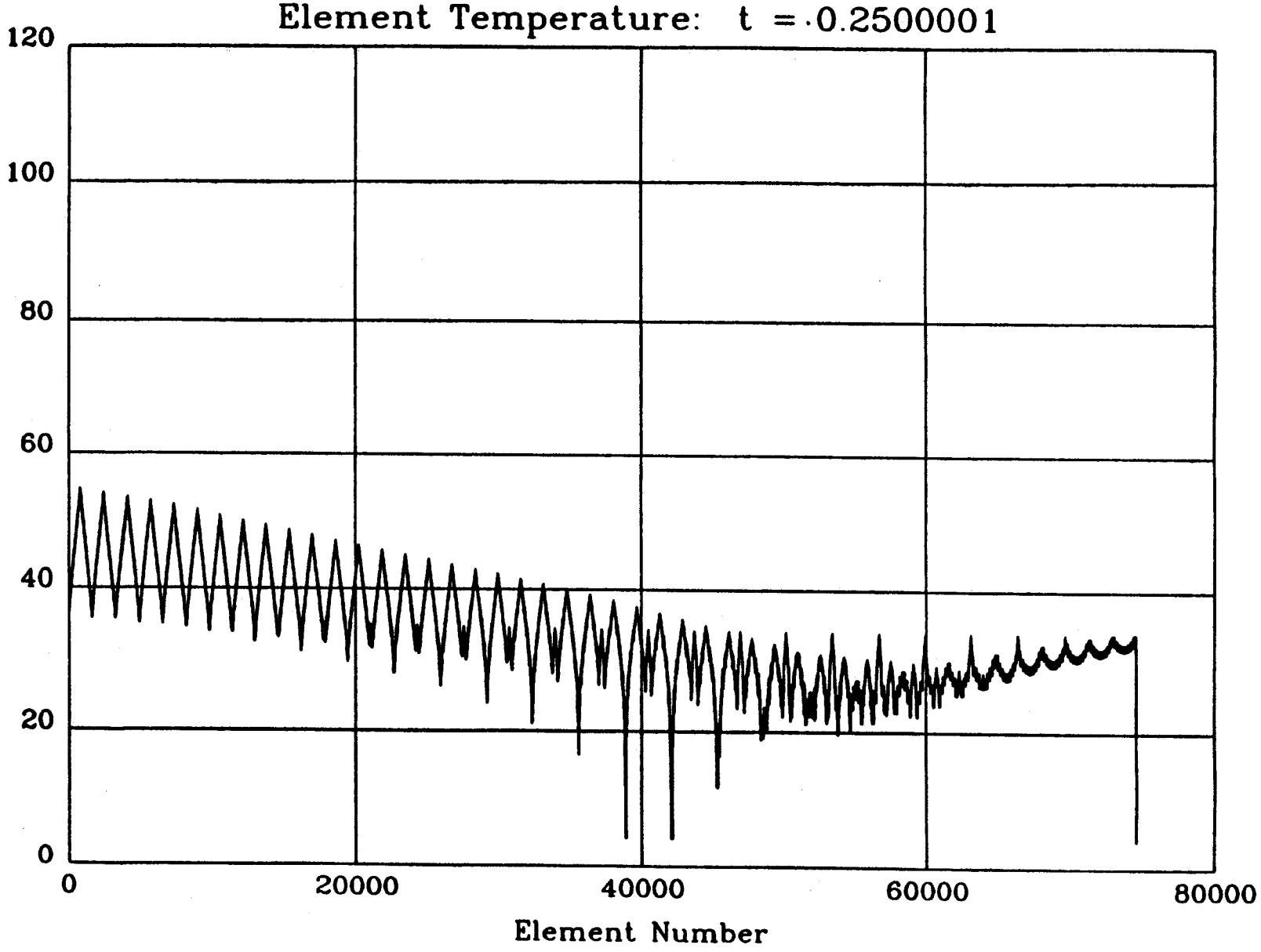

Figure 2–9
Temperature vs Element Number at t = 250 ms

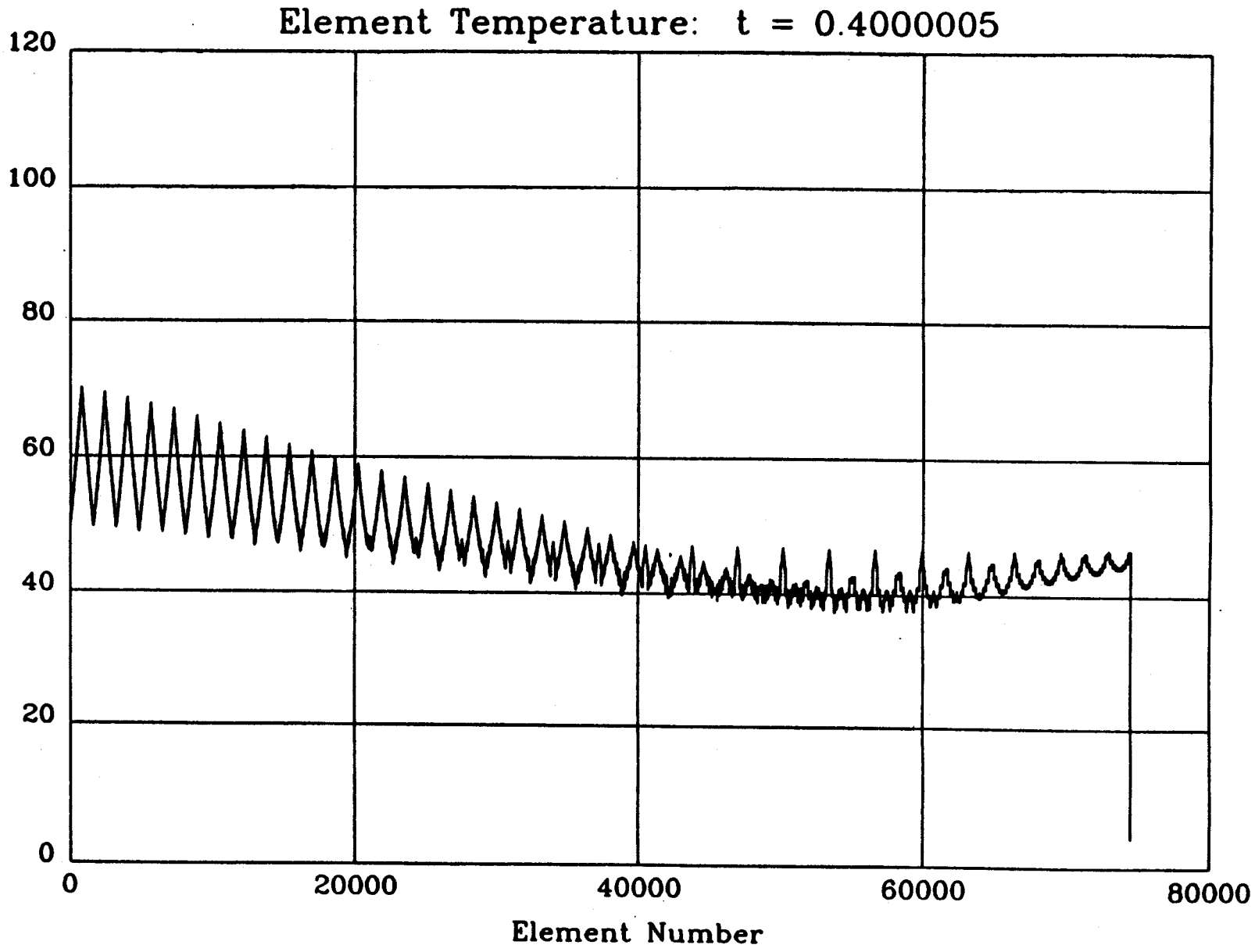

Figure 2–10
Temperature vs Element Number at t = 400 ms

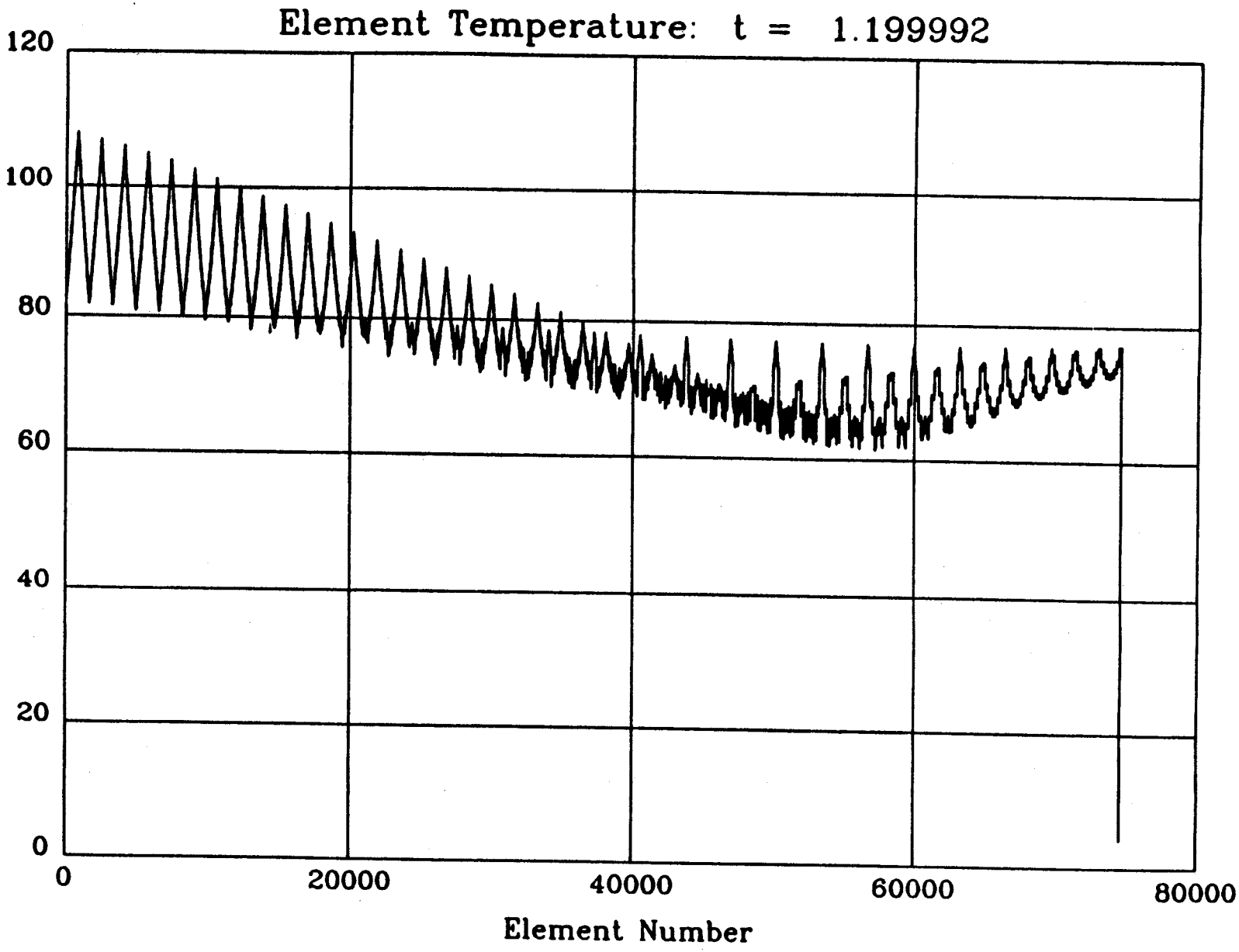

Figure 2–11

Temperature vs Element Number at t = 1.20 s

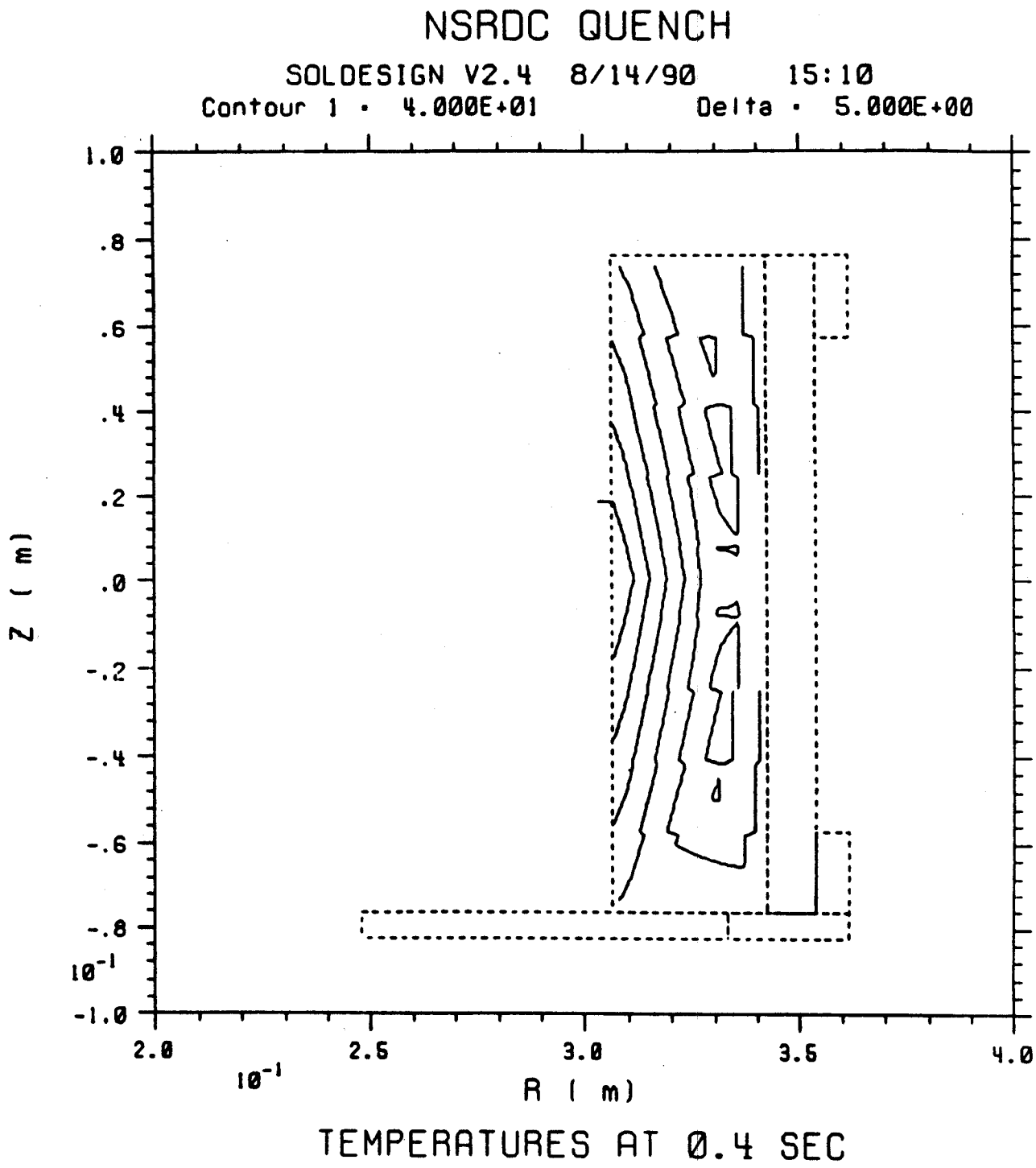

Figure 2–12
Contours of Constant Temperature in the Winding at t = 400 ms

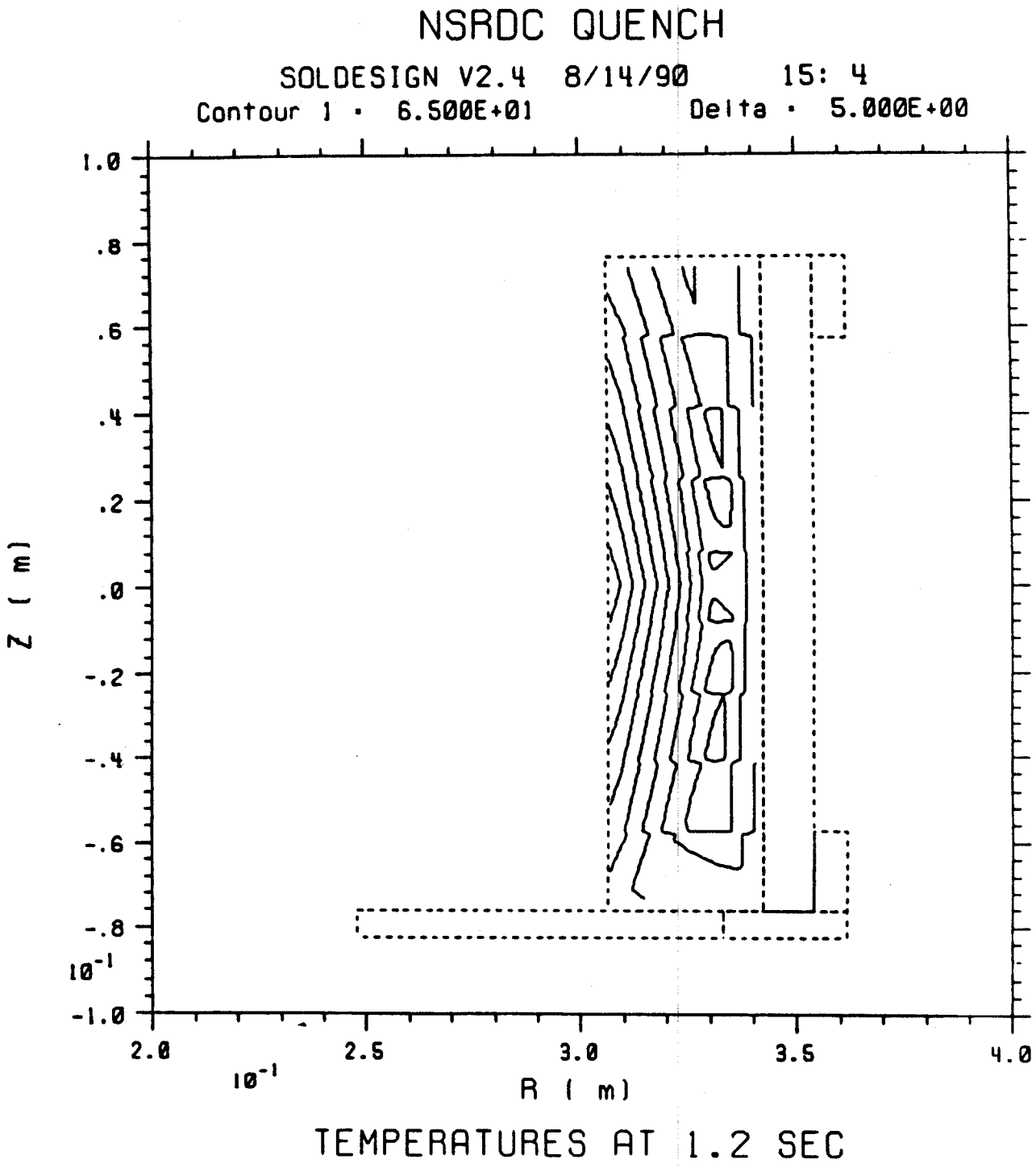

Figure 2–13
Contours of Constant Temperature in the Winding at t = 1.2 s

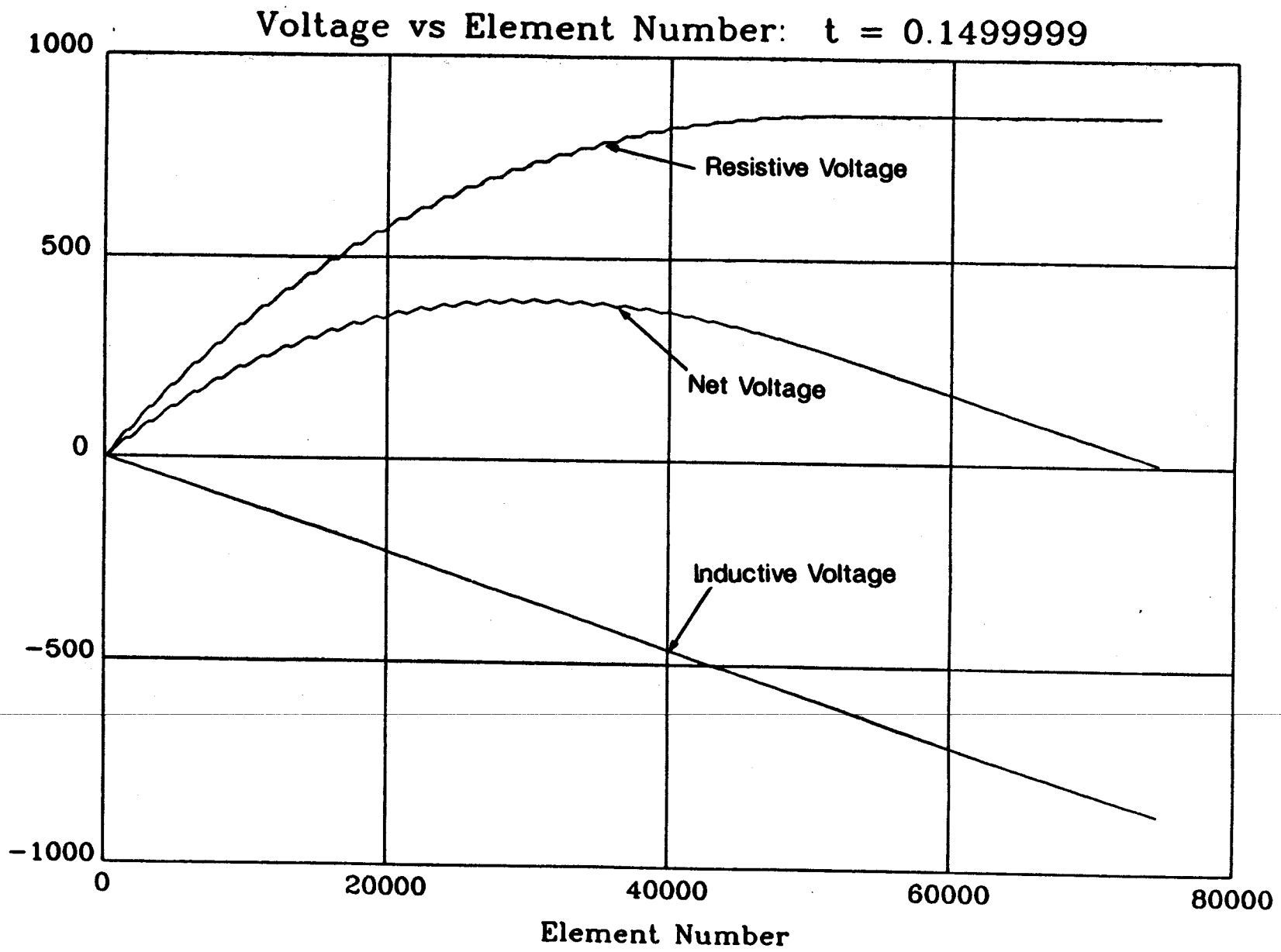

Figure 2–14
Computed Voltage Distributions at t = 150 ms

3.0 ICCS Conductor Stabilization and Quench

3.1 Introduction

Internally Cooled Cable Conductor analyses are complicated by the fact that the processes are highly nonlinear and dependent on induced flow velocities in the helium in the conductor conduit. Stability is typically determined by processes occurring on the millisecond time scale. Quench phenomena of interest, on the other hand, typically occur on the time scale of many seconds or longer. The result is that codes which are written to study stability require a great deal of computer time to track the local nonlinear interactions that determine stability and are not appropriate for the longer times necessary for quench analysis.

In FY90, we surveyed the codes currently available at MIT to analyze problems of this type. We then concentrated on two codes: HESTAB[1], a zero-dimensional model and CICC, a one-dimensional model. Many of the features of these codes are described in this section. We have begun to apply these codes to selected test cases and will pursue their modification and integration into a quench code for ICCS in FY91.

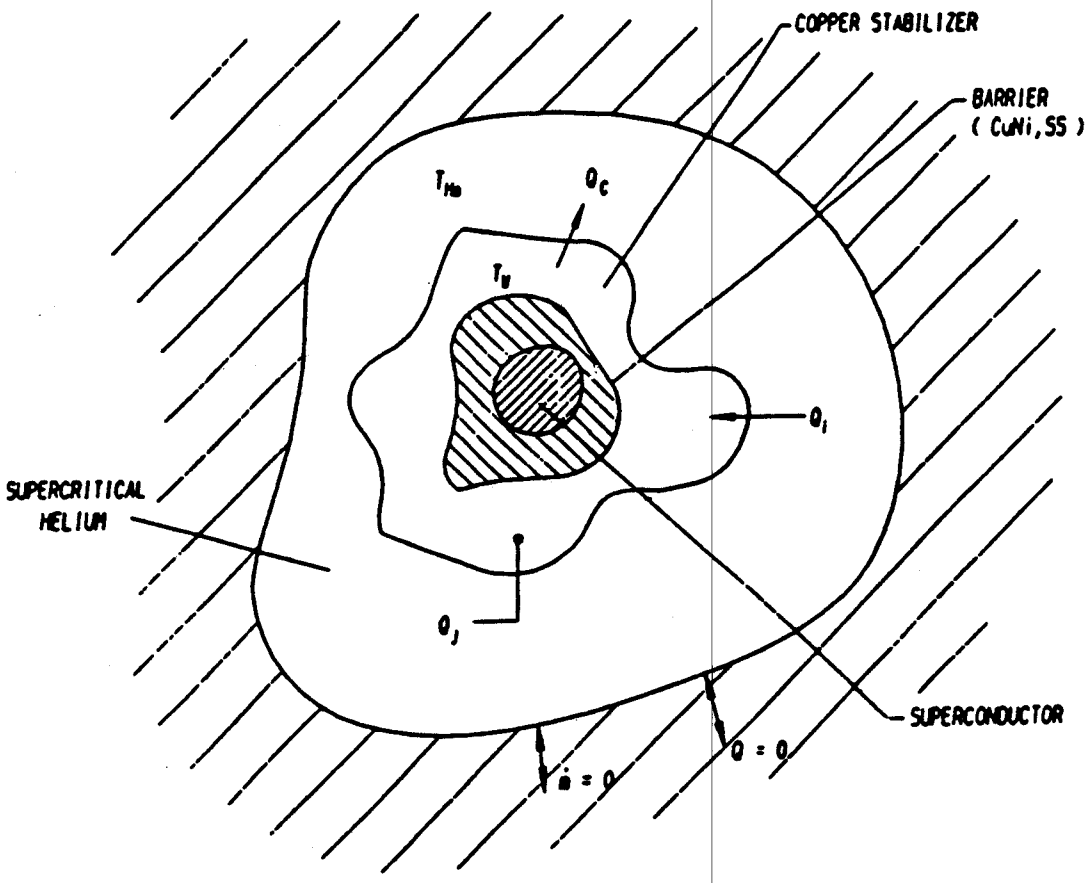

Figure 3.1: Cable-In-Conduit Schematic Modeled by HESTAB (from Reference [11]).

3.2 Description of Codes

3.2.1 HESTAB

HESTAB is a zero dimensional stability code for analysis of cable-in-conduit conductors [10]. The main assumption of the 0-D model is the axial length independency of the problem, which would hold for the first few milliseconds of the recovery process. It is also assumed that no radial temperature gradient exists within the wire, which consists of superconductor, copper and structural jacket (stainless steel). Figure 3.1 shows the system under consideration, which is composed of the wire and supercritical helium. For the superconductor, HESTAB will allow the user to choose between Nb_3Sn and $NbTi$. The stabilizer must be copper and the jacket or barrier must be 304 stainless steel. The property routines are supplemented in two separate programs, program MATPROP is used to evaluate the properties of the wire components, and HEPROP is used to evaluate the helium properties. MATPROP may be modified to simulate systems composed of materials other than the ones mentioned here.

As shown in Figure 3.1 the system as a whole is assumed adiabatic. The specific

heat and thermal conductivities of all material, other than superconductor, copper, helium, and the jacket are considered negligible. The power balance in the conductor referred to the unit length is

$$\dot{Q}_n = \dot{Q}_i + \dot{Q}_j - \dot{Q}_c \tag{3.1}$$

where $\dot{Q}_i$ is the imposed perturbation heat input, $\dot{Q}_j$ is the Joule heating, $\dot{Q}_c$ is the heat removed by the helium at the wire surface and $\dot{Q}_n$ is the net heat input to the wire. The heat removed by the helium is given by

$$\dot{Q}_c = ph(T_w - T_{He}) \tag{3.2}$$

where p is the cooled perimeter, T_w is the wire temperature, T_{He} is the helium temperature, and h is the heat transfer coefficient as given in appendix A.

The governing differential equations are

$$\frac{dT_w}{dt} = \frac{\dot{Q}_n}{A_w C_{pw}} \tag{3.3}$$

$$\frac{dH_{He}}{dt} = \dot{Q}_c \tag{3.4}$$

where A_w is the wire cross-sectional area, C_{pw} is the wire specific heat averaged over the mass weighted wire components (S.C. + Cu + jacket), and H_{He} is the helium enthalpy. HESTAB will allow the user to include any fraction of the structural jacket in the calculation of C_{pw} (see Table 12 under WT).

In order to solve equations (3) and (4) it should first be noted that the helium temperature is an unknown and a function of the enthalpy. The authors have assumed the process to be of constant helium density, thus giving the third required equation to solve the system. The basis for this assumption has been the good correlation of the results obtained by HESTAB with the experimental data [10]. In order to account for this assumption, the authors have used helium enthalpy in lieu of internal energy in equation (4), even though internal energy is thermodynamically more correct for heating a closed fixed volume.

The Joule heating term is given by

$$\dot{Q}_j = \frac{I^2 \rho}{A_{cu}} f \tag{3.5}$$

with I being the operating current which is kept constant in the process, ρ the copper resistivity (including magnetoresistivity) which is also kept constant, A_{cu} the copper cross-sectional area, and

$$f = \begin{cases} 0 & \text{if } T_w < T_{cs}\,; \\ \frac{T_w - T_{cs}}{T_c - T_{cs}} & \text{if } T_{cs} \leq T_w \leq T_c\,; \\ 1 & \text{if } T_w > T_c\,. \end{cases}$$

In the above expression, T_c is the critical temperature of the superconductor which is an input to the program and is kept constant in the recovery process, and T_{cs} is the current sharing temperature given by

$$T_{cs} = T_c - \left(\frac{I}{I_c}\right)(T_c - T_b) \tag{3.6}$$

where I_c is the critical current, and T_b is the helium bath temperature. Equation (6) is based on the assumption that the critical current decreases linearly with increasing temperature.

HESTAB is capable of two modes of operation; 1) the temperature vs. time mode, which determines T_w and T_{He} vs. time for a given input value of $\dot{Q}_i$, and 2) the energy margin mode, that determines the limiting imposed energy in the recovery process as a function of I. The criteria for determining the energy limit corresponding to the recovery/quench boundary are:

1) If $T_{He} \geq T_{cs} \longrightarrow$ Quench
2) If $t > \tau$ and $\frac{dT_w}{dt} \geq 0 \longrightarrow$ Quench
3) If $t > \tau$ and $T_w \leq T_{cs} \longrightarrow$ Recovery

where τ is the pulse time that is an input parameter to the program. The imposed heat is given by $\dot{Q}_i = E/\tau$ for $t < \tau$, and by $\dot{Q}_i = 0$ for $t > \tau$. In mode 2 of the program the limiting value of E (mJ/cm^3 of S.C. + Cu) is determined such that the conductor recovers (for the method used to find E see Table 9 under column 5). In mode 1, HESTAB is given a value of E (mJ/cm^3 of S.C. + Cu) which is then used to obtain the temperature distributions.

With the assumptions made in the 0-D model, it is imperative to realize that the model and hence the code are only valid within a range of a few tens of milliseconds, after which the zero dimensionality of the problem is no longer sustained. The temperature vs. time mode should be used with this notion in mind.

One of the features of HESTAB is its ability to model the induced flow which in turn is used to determine the heat transfer coefficient. The expression used in determining the induced velocity is given in appendix B. The induced flow is responsible for the "dual stability margin" [9], and the program can be used to simulate this margin [10]. HESTAB is capable of finding only one value of E per operating current. When dealing with "dual margins", the user must use the temperature vs. time mode to determine

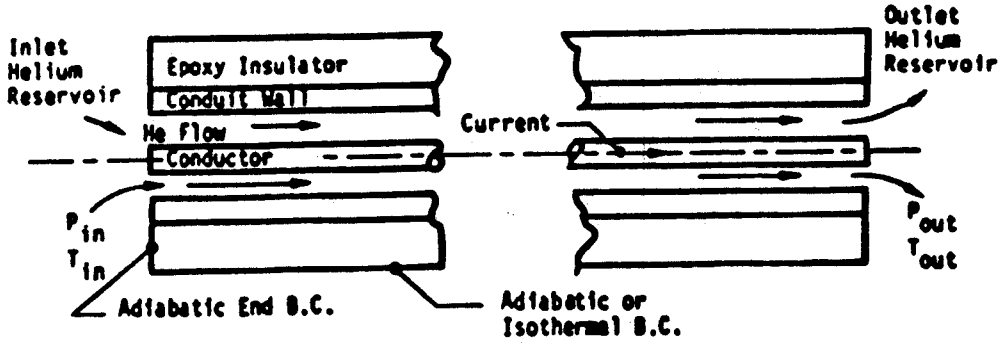

Figure 3.2: Cable-In-Conduit Schematic Modeled by CICC (from Reference [14]).

values of E that are not found by the energy margin mode of the program. This is done by scanning a range of energy (E) and observing the temperature distributions of the conductor. These temperature distributions will then indicate whether the conductor is recovering or quenching.

Included in the appendices is a list of the input parameters to HESTAB with their respective descriptions (see appendix C).

3.2.2 CICC

CICC is a one dimensional quench code that is documented in references [14,15]. The method of solution of the governing equations will not be discussed here and only a brief explanation of the theoretical model will be given below. In solving the 1-D model, the accuracy of the results and the CPU time are dependant on the chosen method of solution. In the case of helium, large variations in the material properties give rise to very long run-times of the 1-D codes.

CICC models the forced flow helium cooled conductor shown in Figure 3.2. The main features of CICC are as follows:

1 CICC uses the SI unit system for all the variables and parameters. The governing differential equations describing the cable-in-conduit are:

a The system of partial differential equations for the single phase helium is

ρ	helium density
u	helium velocity
p	helium pressure
f	Darky friction factor
d_h	hydraulic diameter
e	helium internal energy
T	helium temperature
T_c	conductor (S.C. + Cu) temperature
T_w	conduit wall temperature
k	helium thermal conductivity
A_c	cross sectional area of helium flow channel
A_{tc}	convection heat-transfer perimeter for the conductor
A_{tw}	convection heat-transfer perimeter for the conduit wall
R_c	$\frac{1}{h_c} + \frac{\delta_c}{2k_c}$
R_w	$\frac{1}{h_c} + \frac{\delta_w}{2k_w}$
h_c	helium convection heat-transfer coefficient
δ_c	wall thickness of the conductor
k_c	conductor thermal conductivity
δ_w	conduit wall thickness
k_w	conduit wall thermal conductivity

Table 3.1: Definition of The Variables and The Notation Used in Equations (7-9).

$$\frac{\partial \rho}{\partial t} = -\frac{\partial(\rho u)}{\partial x} \qquad (continuity) \tag{3.7}$$

$$\frac{\partial(\rho u)}{\partial t} = -\frac{\partial}{\partial x}\left(p + \rho u^2\right) - \left(\frac{f}{d_h}\right)\left(\frac{\rho u|u|}{2}\right) \qquad (momentum) \tag{3.8}$$

$$\frac{\partial}{\partial t}\left[\rho\left(e + \frac{u^2}{2}\right)\right] = -\frac{\partial}{\partial x}\left\{(\rho u)\left[\left(e + \frac{p}{\rho}\right) + \frac{u^2}{2}\right]\right\} + \frac{\partial}{\partial x}\left[k\left(\frac{\partial T}{\partial x}\right)\right] + \frac{1}{A_c}\left[\frac{A_{tc}}{R_c}(T_c - T) + \frac{A_{tw}}{R_w}(T_w - T)\right] \qquad (energy) \tag{3.9}$$

with the notation given in Table 1. Note that in this section of the paper the conductor is referred to as superconductor plus the copper.

ρ_c	conductor density
C_c	conductor heat capacity
f_{Cu}	volume fraction of copper in the conductor
A_{cc}	conductor cross-sectional area
Q_{gen}	conductor heat generation which consists of 1. Background nuclear heating 2. Background eddy-current heating 3. Initiating heat pulse 4. Normal-conductor electrical-resistance heating

Table 3.2: Definition of The Variables and The Notation Used in Equation (10).

b The governing equation for the conductor (S.C. + Cu) is

$$(\rho_c C_c)\left(\frac{\partial T_c}{\partial t}\right) = \frac{\partial}{\partial x}\left[f_{Cu}k_{Cu}\left(\frac{\partial T_c}{\partial x}\right)\right] + \frac{1}{A_{cc}}\left[\frac{A_{tc}}{R_c}(T - T_c)\right] + Q_{gen} \tag{3.10}$$

where the notation is given in Table 2, and the value of $\rho_c C_c$ is given by (the subscript 'SC' stands for superconductor)

$$\rho_c C_c = f_{Cu}(\rho_{Cu}C_{Cu}) + (1 - f_{Cu})(\rho_{SC}C_{SC}). \tag{3.11}$$

Note that the value of $f_{Cu}k_{Cu}$ is used in the heat conduction term of equation (10). The actual term for the thermal conductivity of the conductor includes both thermal conductivities of copper and superconductor multiplied by their respective fractions in the conductor. However, the thermal conductivity and the fraction of the superconductor are much smaller than that of copper, so that their product is negligible when calculating the thermal conductivity of the conductor.

c The equation describing the conduit wall is

$$(\rho_w C_w)\left(\frac{\partial T_w}{\partial t}\right) = \frac{\partial}{\partial x}\left[k_w\left(\frac{\partial T_w}{\partial x}\right)\right] + \frac{1}{A_{cw}}\left\{\frac{A_{tw}}{R_w}(T - T_w) + \frac{(A_{te})_1}{(R_e)_1}\left[(T_e)_1 - T_w\right]\right\} \tag{3.12}$$

with the notation given in Table 3.

ρ_w	conduit wall density
C_w	conduit wall heat capacity
$(T_e)_1$	first epoxy sub-layer temperature
A_{cw}	conduit wall cross-sectional area
$(A_{te})_1$	conduit wall to first epoxy sub-layer-interface perimeter
$(R_e)_1$	$\frac{\delta_w}{2k_w} + \frac{(\delta_e)_1}{2k_e}$
$(\delta_e)_1$	wall thickness of the first epoxy sub-layer
k_e	epoxy thermal conductivity

Table 3.3: Definition of The Variables and The Notation Used in Equation (12).

d CICC allows the epoxy layer to be broken up into sub-layers, and in effect solves the 2-D problem for the epoxy layer. The energy equation for the first sub-layer of the epoxy (the sub-layer next to the conduit wall) is

$$(\rho_e C_e)\left(\frac{\partial (T_e)_1}{\partial t}\right) = \frac{\partial}{\partial x}\left[k_e\left(\frac{\partial (T_e)_1}{\partial x}\right)\right] + \frac{1}{(A_{ce})_1}\left\{\frac{(A_{te})_1}{(R_e)_1}\left[T_w - (T_e)_1\right] + \frac{(A_{te})_2}{(R_e)_2}\left[(T_e)_2 - (T_e)_1\right]\right\} \tag{3.13}$$

where the notation is given in Table 4.

e The equation describing all sub-layers except the inner or the outer most sub-layers is

$$(\rho_e C_e)\left(\frac{\partial (T_e)_n}{\partial t}\right) = \frac{\partial}{\partial x}\left[k_e\left(\frac{\partial (T_e)_n}{\partial x}\right)\right] + \frac{1}{(A_{ce})_n}\left\{\frac{(A_{te})_n}{(R_e)_n}\left[(T_e)_{n-1} - (T_e)_n\right] + \frac{(A_{te})_{n+1}}{(R_e)_{n+1}}\left[(T_e)_{n+1} - (T_e)_n\right]\right\} \tag{3.14}$$

with notation given in Table 4.

f For the outer most epoxy sub-layer two boundary conditions are allowed by CICC (isothermal or adiabatic). The isothermal boundary condition will use equation (14) to describe this sub-layer, with the term $(T_e)_{n+1}$ replaced by T_o, where T_o is the temperature (T_{in}) of the high pressure (p_{in}) reservoir. The value of $(R_e)_{n+1}$ in this

ρ_e	epoxy density
C_e	epoxy heat capacity
$(T_e)_2$	second epoxy sub-layer temperature
$(A_{ce})_1$	first epoxy sub-layer cross-sectional area
$(A_{te})_2$	first to second epoxy sub-layer perimeter
$(R_e)_2$	$\frac{(\delta_e)_1}{2k_e} + \frac{(\delta_e)_2}{2k_e}$
$(\delta_e)_2$	wall thickness of the second epoxy sub-layer
$(T_e)_n$	nth epoxy sub-layer temperature
$(R_e)_n$	$\frac{(\delta_e)_{n-1}}{2k_e} + \frac{(\delta_e)_n}{2k_e}$
$(\delta_e)_n$	wall thickness of the nth epoxy sub-layer

Table 3.4: Definition of The Variables and The Notation Used in Equations (13,14).

case is given by $(R_e)_{n+1} = \frac{(\delta_e)_n}{2k_e}$. In the adiabatic boundary condition this sub-layer is described by equation (14) with the second term inside the bracket ({}) omitted. Boundary conditions used by CICC will be discussed further in section 2.

2 Boundary conditions used by CICC are:

a There are two types of boundary conditions for the helium momentum equation. If the flow is not choked, the static pressure at the two ends of the flow channel are used as boundary conditions for the helium pressure. If the flow is choked at an exit (note that for a constant area duct flow, choking can only occur at an exit) then the helium velocity is set equal to the sonic velocity at that exit, and the pressure corresponding to a Mach number of 1 is used as a boundary condition for the helium pressure.

b For the helium energy equation the enthalpies at the ends of the channel are set equal to the enthalpies of the reservoirs. The conductor, conduit wall and the epoxy are all assumed adiabatic at the ends of the channel. The outer epoxy surface can be either adiabatic or isothermal. The equations describing the outer sub-layer of the epoxy for both type of boundary conditions are given in section 4-f.

3 CICC runs in two stages:

a Given the pressures and the temperatures of the two reservoirs, at the two ends of the channel, CICC will start to solve for the steady state solution. This requires solving the transient problem of the conductor until steady state is reached. The Joule

heating term and the initiating heat pulse are not included in this stage of the problem (Q_{gen} term includes only the background nuclear and the background eddy-current heating terms). When it is determined that the variables are time independent the program will advance to the next level of operation.

b The second mode of operation involves solving the conductor stability or quench problem. In this part an initiating heat pulse will start the process, and the Joule heating of the conductor is now taken into account.

4 CICC models the conductor (flow channel) as being composed of a number of turns; with the number of turns being an input parameter to the program. This allows CICC to model the nuclear heating and the magnetic field of a coil.

5 The heat generation (Q_{gen}) used in equation (10) includes 4 terms:

a For each turn of the conductor, the background nuclear heating term is a trapezoidal profile in space. The four values of the coil-turn lengths that are the coordinates of this trapezoidal profile are inputs to the program. This profile is an exponentially decaying function of space across the conductor (from turn to turn) with the exponential time-constant being an input to CICC. The nuclear heating term is a constant in time and is always present in the problem (both in obtaining the steady state solution and in the conductor quench, or recovery problem).

b The background eddy-current heat load is an input to CICC that is constant in both time and space. This term is present across the whole conductor during the entire problem (both in obtaining the steady state solution and in the conductor quench, or recovery problem).

c The initiating heat pulse has a rectangular profile in space. CICC is given the beginning and the ending lengths of the conductor (flow channel) at which this heat pulse is located. The pulse starts after the steady state solution of the conductor has been obtained, and is a constant in time. The time at which this pulse drops to zero (measured from the time the pulse starts) is an input to the program.

d The Joule-heating term (normal-conductor electrical-resistance heating) is due to the resistance of the stabilizer (copper) and the current in the conductor. The value of the current can be varied in time. A value of a voltage drop (Voltci) is an input to CICC, with the current being a constant in time until this voltage is reached across the conductor. When this voltage is reached the current becomes an

exponentially decreasing function of time, with the exponential time-constant (external dump resistor) being an input to the program.

6 The correlations for the friction factor and the heat transfer coefficient used in CICC are:

a For the friction factor, the user is given a choice between correlations given by Hooper [6] and Van Sciver [13]. The correlation given by Hooper is

$$f = 64/Re \qquad (for\ \ Re < 99.73) \tag{3.15}$$

$$ln(f/4) = 13.15Re^{-0.36} - 4.338 \qquad (for\ \ Re > 99.73) \tag{3.16}$$

The Van Sciver correlation is given by

$$f = 64/Re \qquad (for\ \ Re < 10) \tag{3.17}$$

$$ln(f/4) = -0.6760ln(Re) + 2.027 \qquad (for\ \ 10 < Re < 10^4) \tag{3.18}$$

$$ln(f/4) = 1144Re^{-0.7741} - 5.116 \qquad (for\ \ Re > 10^4) \tag{3.19}$$

b The heat transfer coefficient used in CICC contains a steady state term [4,5], and a transient term [1]. The steady state part is given by

$$Nu = 0.0259Re^{0.8}Pr^{0.4}(\frac{T_w}{T})^{-0.716} \tag{3.20}$$

where Nu is the Nusselt number ($(h_c)_{ss}k/d_h$), Pr is the Prandlt number ($\mu C_p/k$), and T_w is the temperature of the material adjacent to the helium. The transient part of the heat transfer coefficient is

$$(h_c)_t = 0.5\left(\frac{\pi k \rho C_p}{t}\right)^{1/2} \tag{3.21}$$

where all the properties correspond to that of helium, with k being the thermal conductivity, ρ the density, and C_p the specific heat at constant pressure. The heat transfer coefficient is then given by

$$h_c = (h_c)_t + (h_c)_{ss} \tag{3.22}$$

where $(h_c)_{ss}$ is the steady state heat transfer coefficient as determined by equation (20).

7 CICC models the magnetic field across each turn as a trapezoidal shape in space, and a constant in time. The locations of the coil-turn lengths that are the coordinates for the trapezoidal magnetic field profile are inputs to CICC. Across each turn the magnetic field is in a form of a trapezoid, with the maximum and the minimum fields (B_{max}, B_{min}) being inputs to the program.

8 CICC allows the user to choose different mesh sizes in both time and space, allowing the problem to be analyzed in more detail for chosen regions of space and time.

9 The procedure for running CICC on the Cray is given in reference [15]. Once the cosmos file, the source code, and the graphics program are present, the command "cosmos i=ccicc / t v" will start the CICC operation on the Cray. The input files are:

a NNNN50 is the input file for CICC, where "NNNN" is a chosen four character name of the file, and "50" is a number that must be present in the name of the input file. The format of this file is explained in reference [15].

b NNNN50pi is the input file for the graphics program which complements CICC. The format of this file is also explained in reference [15].

Appendix A

Heat Transfer Coefficient Used in HESTAB

The heat transfer coefficient which HESTAB uses is composed of three terms [1]:

1 The transient heat transfer coefficient is based on modeling helium as a semi-infinite body with an imposed step in temperature T_w, at the wire interface. Assuming the wire temperature to be constant and neglecting the convective heat transport, an expression can be found for the transient heat transfer coefficient;

$$h_t = \frac{1}{2}\left(\frac{\pi k \rho C_p}{t}\right)^{1/2} \tag{A.1}$$

where all the properties correspond to that of helium, with k being the thermal conductivity, ρ the density, and C_p the specific heat at constant pressure. The constant wall temperature imposed on the helium/wire boundary is not realistic. An alternative expression could be obtained using the constant heat flux boundary condition at the interface, with the resulting expression being $\pi/2$ times that given in equation (29). HESTAB will allow the user to choose between the two models mentioned here (see NVARH in the list of HESTAB inputs). The results on the energy margin are very much the same when using either of the two expressions.

2 The Kapitza conductance is given by

$$h_k = 200(T_w + T_{He})(T_w^2 + T_{He}^2) \tag{A.2}$$

For more details on this expression refer to [1].

3 The steady state component is

$$h_s = 0.023\frac{k}{d_h} Re^{0.8} Pr^{0.4} y \tag{A.3}$$

which is a modified form of the Dittus-Boelter expression; with $y = \frac{1+0.4z-(1+0.8z)^{0.5}}{0.08z^2}$, $z = \beta(T_w - T_{He})$, where $\beta = \frac{1}{\rho}\left(\frac{\partial \rho}{\partial T}\right)_p$ is the coefficient of thermal expansion of helium.

The total heat transfer coefficient is then given by

$$h = h_s + \frac{h_t h_k}{h_t + h_k}. \tag{A.4}$$

Appendix B

The Induced Velocity Used in HESTAB

Based on derivations and models given in references [3] and [10], HESTAB uses the following relation to obtain the induced velocity:

$$\frac{dV_i}{dt} = \frac{c\beta\dot{Q}}{2A\rho C_p} - 2f\frac{V_i^2}{d_h} \tag{B.1}$$

where V_i is the induced velocity, c is the speed of sound in helium, $\beta = \frac{1}{\rho}(\frac{\partial\rho}{\partial T})_p$ is the coefficient of thermal expansion of helium, A is the cross-sectional flow area, ρ is the helium density, C_p is the helium specific heat at constant pressure, d_h is the hydraulic diameter of the flow channel, f is the friction factor as given in Table 12 (under FCORR), and $\dot{Q}$ is the input heat to the helium (HESTAB offers two choices for $\dot{Q}$, see Table 11 under NVELC).

The expression given by equation (33) is valid for regions where $\dot{Q}$ is not zero (since $\dot{Q}$ could be a function of space), and in regions where $\dot{Q} = 0$ this expression must be modified. For $0 \leq t \leq l/c$, the induced velocity is obtained using equation (33), and for $t > l/c$ the value of V_i obtained by equation (33) must be multiplied by l/ct, where l is the length of the heated section.

The total helium velocity is composed of the induced and the steady state velocities, and is given by

$$V_{tot} = \frac{(V_{ss} + 0.5V_i) + |V_{ss} - 0.5V_i|}{2} \tag{B.2}$$

Appendix C

List of The Inputs to HESTAB

The full list of all the input data to HESTAB, their type in Fortran language (e.g. character type), and their units is given in tables 11-13. A few notes have to be made about the program:

1 The input file is for015.dat .

2 The output files are:

a for016.dat which contains the echo of the input and the iteration results. The output in this file will be clear, once viewed by the user.

b for017.dat which contains columns used for plotting (by the user). The output of this file is not clear and is given in tables 9 and 10.

3 The file for002.dat contains errors and warnings (if any), created by the IMSL routine that is used in HESTAB. The user must always check this file before reviewing any of the results. The definition of the warnings and errors in this file are given in the IMSL library [7].

4 Typical run times of HESTAB, on the VAX, range between minutes to hours, depending on the system under consideration.

TEMPERATURE VS. TIME MODE	
column 1	time (sec)
column 2	T_w (K)
column 3	T_{He} (K)
column 4	$\dot{Q}_j$ $(watts/m)$
column 5	$\dot{Q}_c$ $(watts/m)$
column 6	$\dot{Q}_n$ $(watts/m)$
column 7	$\dot{Q}_i$ $(watts/m)$
column 8	helium pressure (atm)
column 9	heat transfer coefficient (watts/K-cm^2)
column 10	helium velocity (cm/sec)

Table C.1: Description of The Output of HESTAB (file for017.dat) in The Temperature Vs. Time Mode.

ENERGY MARGIN MODE	
column 1	$\frac{I}{I_c}$ (I = operating current, and I_c = critical current at normal operating condition)
column 2	current density using $\frac{I}{A_{overall}}$, $(amps/cm^2)$ (where $A_{overall}$ is an input explained in the HESTAB input lists under AOVRL)
column 3	current density using $\frac{I}{A_{front}}$, $(amps/cm^2)$ (where A_{front} is an input explained in the HESTAB input lists under AFRNT)
column 4	$E_{max}(mJ/cm^3$ of Cu + S.C.), is equal to the total enthalpy change of the wire (S.C. + Cu + jacket) plus the helium from bath temperature to $T_w(t)$; noting that the enthalpy of the jacket is multiplied by WT (see HESTAB inputs under WT)
column 5	E (mJ/cm^3 of Cu + S.C.) which is the energy margin for recovery, $(\dot{Q}_i = E/\tau)$ (the value of E is determined using the following logic: if for a given E the conductor recovers replace E_{min} by E, otherwise (conductor doesn't recover) replace E_{max} by E, this process continues until the difference between E_{max} and E_{min} is less than 4%)
column 6	$E_{min}(mJ/cm^3$ of Cu + S.C.), which is similar to E_{max} except that no helium is included in calculation of E_{min}
column 7	δ (%), which is the percent difference between E_{min} and E_{max} when the value of E is obtained, so that the exact value of E will lie within + or - δ of the energy margin (E) found by HESTAB

Table C.2: Description of The Output of HESTAB (file for017.dat) in The Energy Margin Mode.

NAME (CH*80)	name of the problem
TITLE (CH*80)	title of the problem
NSOL (I*4)	operation mode. 0-energy margin mode 1-temperature vs. time mode
NVARH (I*4)	variable heat transfer coefficient 0-no 1-yes (using h_t given by equation (29) in appendix A) 1-yes (using $\pi/2$ times equation (29) for h_t)
NVELC (I*4)	variable velocity 0-no 1-yes (using $\dot{Q}_c$ for $\dot{Q}$ in equation (33)) 2-yes (using $\dot{Q}_i$ for $\dot{Q}$ in equation (33))
NCHECK (I*4)	recovery check during temp. vs. time mode so that the program will stop when the conductor has been determined to be recovering (not used in energy margin mode) 0-no 1-yes
NGRAPH (I*4)	graphic output file (for017.dat) 0-no 1-yes
NDET (I*4)	detailed iteration output (for016.dat) 0-no 1-yes
NINTR (I*4)	interactive run 0-no 1-yes
ISCTYP (I*4)	superconductor type 1-Nb_3Sn 2-$NbTi$

Table C.3: List of HESTAB Inputs.

ASC (R*4)	cross-sectional area of superconductor, (cm^2)
RHOSC (R*4)	density of superconductor, (g/cm^3)
TC (R*4)	critical temperature of the S.C. at normal operating conditions, (K)
JC (R*4)	critical current density of the S.C. at normal operating conditions, (amps/cm^2 of S.C.) (kept constant in the process)
ACU (R*4)	cross-sectional area of the copper, (cm^2)
RHOCU (R*4)	density of copper, (g/cm^3)
RRR (R*4)	residual resistivity ratio of copper
ASH (R*4)	cross-sectional area of the jacket, (cm^2)
RHOSH (R*4)	density of jacket, (g/cm^3)
WT (R*4)	fraction of the jacket to be included in calculating the average specific heat of the wire, E_{max}, and E_{min} (value between 0-1)
AOVRL (R*4)	$A_{overall}$ (cm^2), which is the total cross-sectional area of the wire (S.C. + Cu + jacket)
AFRNT (R*4)	A_{front} (cm^2), which is any value of a cross-sectional area that the user feels should be used in calculating the operating current density
XLEN (R*4)	length of the heated zone, (cm)
AHE (R*4)	cross-sectional area of the helium flow channel, (cm^2)
PIN (R*4)	initial helium pressure, (atm)
THEIN (R*4)	initial helium temperature, (K)
AHT (R*4)	heated perimeter, (cm)
DH (R*4)	hydraulic diameter, (cm)
VEL (R*4)	helium velocity at t=0, (cm/sec)
FCORR (R*4)	correction to the Darky friction factor, the value of the friction factor is $f = (\frac{16}{200})(FCORR)$ $(Re < 200)$ $f = (\frac{16}{Re})(FCORR)$ $(200 < Re < 1100)$ $f = (0.0014 + \frac{0.125}{Re^{0.32}})(FCORR)$ $(Re > 1100)$

Table C.4: List of HESTAB Inputs (continued).

B (R*4)	magnetic field, (Tesla)
FCI (R*4)	initial value of $(\frac{I}{I_c})$ in the energy margin mode, (%) (the energy margin in mode 2 of the program is obtained for values of FCI to FCF in steps of FCS, and in mode 1 of the operation the value of the current used in obtaining the temp. distributions is given by FCF)
FCF (R*4)	final value of $(\frac{I}{I_c})$, (%)
FCS (R*4)	$\frac{I}{I_c}$ step, (%)
TAU (R*4)	the time constant (τ) of $\dot{Q}_i$, (sec)
LTYPE (R*4)	only use 2 for step input of $\dot{Q}_i$
STEP (R*4)	integration time step, which must be less than τ, (sec)
PSTEP (R*4)	print-out time step for temp. vs. time in the file for016.dat, (sec) (not used in the energy margin mode)
GSTEP (R*4)	print-out time step for temp. vs. time in the file for017.dat, (sec) (not used in the energy margin mode)
TMAX (R*4)	time limit for the temp. vs. time mode, (sec) (not used in the energy margin mode)
EO (R*4)	the value of E used in $\dot{Q}_i = \frac{E}{\tau}$,(mJ/cm^3 of S.C. + Cu). HESTAB uses this in temp. versus time mode (not used in the energy margin mode)

Table C.5: List of HESTAB Inputs (continued).

Bibliography

[1] Arp, V. D., "Stability and Thermal Quenches in Forced-Cooled Superconducting Cables", *Proc. of 1980 Superconducting MHD Magnet Design Conference*, 142, MIT, 1980.

[2] Dresner, L., "Superconductor stability, 1983: a review", *Cryogenics*, pp.283-292, June 1984.

[3] Dresner, L., "Thermal Expulsion of Helium From a Quenching Cable-In-Conduit Conductor", in *Proceedings of The Ninth Symposium on The Engineering Problems of Fusion Research Chicago, 1981*, IEEE Publication No. 81CH1715-2NPS, pp. 618-621.

[4] Giarratano, P. J., Arp, V. D. and Smith, R. D., "Forced Convection Heat Transfer to Supercritical Helium", *Cryogenics*, 11, pp 385-393, 1971.

[5] Giarratano, P. J., Hess, R. C. and Jones, M. C., "Forced Convection Heat Transfer to Subcritical Helium I", *Advances in Cryogenic Engineering*, Vol. 19, Sec. K-1, 1974.

[6] Hooper, R. J., "Friction Factor Correlations for Cable-In-Conduit Conductors", memo. FEDC-M-84-E/M-016, Fusion Engineering Design Center, Oak Ridge National Laboratory, March 5, 1984.

[7] IMSL Documentation, Version 9.2 .

[8] Lubell, M. S., "Empirical Scaling Formulas For Critical Current And Critical Field For Commercial NbTi", IEEE Transaction on Magnetics, Vol. MAG-19, No. 3, May 1983.

[9] Lue, J. W., Miller, J. R. and Dresner, L., "Stability of Cable-In-Conduit Superconductors", *J. Appl. Phys.*, 51(1), pp. 772-783, Jan 1980.

[10] Minervini, J. V. and Bottura, L., "Modeling of Transient Stability In Cable-In-Conduit Superconductors", personal communication (to be published), The NET Team, 1990.

[11] Minervini, J. V. and Bottura, L., "Stability Analysis of NET TF and PF Conductors", Internal Report, EUR/FU-XII/80/87/77, October 1987.

[12] SSC Report, Site-Specific Conceptual Design, personal communication, June 1990.

[13] Van Sciver, S. W., private communication with R. L. Wong, University of Wisconsin-Madison, College of Engineering, Applied Superconducting Center, Oct 14, 1988.

[14] Wong, R. L., "Program CICC, Flow And Heat Transfer In Cable-In-Conduit Conductors–Equations & Verification", Lawrence Livermore National Laboratory Internal Report, UCID 21733, May 1989.

[15] Wong, R. L., "Program CICC, Flow And Heat Transfer In Cable-In-Conduit Conductors–User's Manual", Lawrence Livermore National Laboratory Internal Report, UCID 21941, Feb 1990.